

## THE G19.6–0.2 REGION OF STAR FORMATION: MOLECULAR AND IONIZED ENVIRONS

GUIDO GARAY,<sup>1</sup> JAMES M. MORAN,<sup>2</sup> LUIS F. RODRÍGUEZ,<sup>3</sup> AND MARK J. REID<sup>2</sup>

Received 1996 January 19; accepted 1997 August 18

### ABSTRACT

We present VLA observations, made with angular resolutions of 2"–3", of the ionized gas (H66 $\alpha$  recombination line and 1.6 GHz continuum) and of the molecular gas ([2, 2] inversion transition of NH<sub>3</sub>) toward the star formation region known as G19.6–0.2. The observations of the ionized gas indicate the presence of five distinct H II regions that are excited by individual stars, implying the presence of a cluster of O–B stars. Three of the individual H II regions have ringlike structures, with sizes ranging from 0.1 to 0.4 pc, and have clumpy and inhomogeneous distributions of gas. Some of the ultracompact structures detected toward these regions with higher angular resolution ( $\sim 0.^{\circ}4$ ) probably are associated with partially ionized clumps, which are externally ionized, and embedded within larger H II regions. The brightest compact H II region within the complex shows a cometary-like morphology, which may be due to the expansion of ionized gas in an anisotropic medium.

The ammonia observations show that the molecular emission arises from three distinct structures: a dense ( $\sim 9 \times 10^6 \text{ cm}^{-3}$ ) clump, located near the center of the cluster of H II regions, which has a size of  $\sim 0.05$  pc and exhibits very broad line widths ( $\sim 9.5 \text{ km s}^{-1}$ ), and two less dense ( $\sim 1 - 2 \times 10^5 \text{ cm}^{-3}$ ) clumps, one of which is detected in absorption toward the northernmost H II region. The physical relationship between these molecular structures and the ionized gas is discussed. We find that the cometary-like and the most compact H II region within the complex are intimately associated with the densest ammonia clump. The mean velocity of the ionized gas is blueshifted with respect to the mean velocity of the molecular clump by  $3.5 \text{ km s}^{-1}$ . We suggest that the star that excites this H II region was formed at the edge of the densest molecular clump. The ionized gas flowing toward the observer is undergoing expansion into the lower density interclump medium (champagne flow). In the opposite direction, the H II region is driving a shock into the dense molecular clump, compressing it and further increasing its density. The less dense ammonia clumps are probably heated and compressed by the shock fronts driven by the more extended H II regions.

*Subject headings:* H II regions — ISM: individual (G19.6–0.2) — ISM: molecules — ISM: structure — radio lines: ISM — stars: formation

### 1. INTRODUCTION

G19.6–0.2 is a complex region of ionized gas located at a kinematic distance, based on the rotation curve of Brand (1986), of 3.5 kpc (Churchwell, Walmsley, & Cesaroni 1990, hereafter CWC). Radio continuum observations with an angular resolution of  $\sim 2''$  show the presence, within a region of  $\sim 40''$  in diameter, of bright compact components coextensive with larger and weaker components (Ho & Haschick 1981; Garay, Reid, & Moran 1985, hereafter GRM). At higher angular resolution ( $\sim 0.^{\circ}4$ ) the radio observations show the presence of several ultracompact structures with irregular shapes (Wood & Churchwell 1989). The complex contains water masers (Genzel & Downes 1977; CWC) and hydroxyl masers (GRM), indicating that it is an active region of massive-star formation. Single-dish observations of molecular lines with high critical densities show the presence of dense molecular gas with a broad range in velocity (CWC; Plume, Jaffe, & Evans 1992). The observed line widths (FWHM of  $\sim 10 \text{ km s}^{-1}$ ) are considerably greater than the thermal widths, which indicates that nonthermal motions dominate the dense

molecular region. The angular resolution of single-dish observations is, however, inadequate to resolve the spatial and velocity structure of the dense molecular gas. Hence it is not possible with such observations to determine the association between the dense molecular gas and the compact H II regions.

Recent observations (Cesaroni, Walmsley, & Churchwell 1992; Cesaroni et al. 1994; Gómez, Garay, & Lizano 1995) have shown that compact regions of ionized gas are very often associated with dense and warm molecular clumps. The physical nature of these clumps and their intimate association with compact H II regions are, however, not entirely clear. Cesaroni et al. (1994) found that, in three of four cases, the molecular clumps are offset from their companion compact H II regions, and they suggested that molecular gas is warmed by luminous objects other than the star responsible for the excitation of the associated compact H II region. On the other hand, Gómez et al. (1995) investigated other ammonia clumps and found that they are intimately associated with compact H II regions and that their luminosities could be explained as a result of heating by the ionizing star of the H II region. Clearly, more observations are needed to understand fully the physical characteristics of the environment in the immediate vicinity of recently formed massive stars. In particular, to investigate the dynamics of these regions it is essential to measure the velocity field of both the ionized regions and the dense molecular regions. The former can be achieved through observations of hydrogen radio recombination lines and the

<sup>1</sup> Departamento de Astronomía, Universidad de Chile, Casilla 36-D, Santiago, Chile.

<sup>2</sup> Harvard-Smithsonian Center for Astrophysics, 60 Garden Street, Cambridge, MA 02138.

<sup>3</sup> Instituto de Astronomía, UNAM, Apdo. Postal 70-264, México, D.F. 04510, México.

TABLE 1  
SUMMARY OF OBSERVATIONAL PARAMETERS

| Observation                | Frequency (MHz) | Number of Channels | Velocity Resolution (km s <sup>-1</sup> ) | Center Velocity (km s <sup>-1</sup> ) | Velocity Coverage (km s <sup>-1</sup> ) | H II Region | Largest Scale (arcsec) | Synthesized Beam (arcsec) | rms Noise (mJy beam <sup>-1</sup> ) |
|----------------------------|-----------------|--------------------|---|---------------------------------------|---|-------------|------------------------|---------------------------|-------------------------------------|
| H66 $\alpha$ .....         | 22364           | 31                 | 5.25                                      | 51.1                                  | 163                                     | C           | 25                     | 3.6 × 3.1 <sup>a</sup>    | 5.9                                 |
| NH <sub>3</sub> (2, 2).... | 23722           | 63                 | 1.23                                      | 50.0                                  | 78                                      | D           | 60                     | 3.4 × 2.4                 | 7.1                                 |
|                            | 1627            | ...                | ...                                       | ...                                   | ...                                     | A           | 38                     | 1.5 × 1.2                 | 0.3                                 |
|                            | 4995            | ...                | ...                                       | ...                                   | ...                                     | A/B         | 36                     | 1.6 × 1.2 <sup>b</sup>    | 0.9                                 |
|                            | 22372           | ...                | ...                                       | ...                                   | ...                                     | C           | 25                     | 2.5 × 1.9                 | 2.4                                 |

<sup>a</sup> 60 k $\lambda$  taper.

<sup>b</sup> 150 k $\lambda$  taper.

latter through observations of molecular lines with high critical densities. In dense and warm molecular cores the abundance of ammonia is considerably enhanced with respect to that in cooler regions (see Walmsley 1989, 1992). Thus, ammonia lines have proved to be superb tracers of the dense molecular gas around newly formed stars (CWC; Cesaroni et al. 1992). Finally, since the angular size of compact H II regions and dense molecular cores is typically a few arcseconds, observations with high angular resolution are required.

In this paper we report high angular resolution observations of the G19.6–0.2 region of massive-star formation in the H66 $\alpha$  hydrogen radio recombination line, the (2, 2) inversion transition of ammonia, and 1.6 GHz radio continuum, made with a resolution of  $\sim 3''$ . The main goals of this study were to find the location of the dense molecular gas with respect to the massive stars (ultracompact H II regions), and to determine the velocity structure and physical condition of the ionized and molecular components across the whole region. In particular, we wanted to understand the physical and dynamical relationship between the dense, warm molecular gas and the compact H II regions, and the physical basis of the broad molecular-line widths.

## 2. OBSERVATIONS

The observations were made with the Very Large Array (VLA) of the National Radio Astronomy Observatory,<sup>4</sup> with the spectral line system on 1982 January 9 (H66 $\alpha$  line observations) and on 1992 September 14 (NH<sub>3</sub> [2, 2] line observations), and in the continuum mode on 1983 November 12 (1.6 GHz observations). The basic observing parameters are summarized in Table 1.

### 2.1. H66 $\alpha$ Line

The H66 $\alpha$  radio recombination line, which has a rest frequency of 22.364 GHz, was observed with a 12.5 MHz bandwidth and 31 spectral channels spaced at intervals of 0.391 MHz, which provided a velocity resolution of 5.3 km s<sup>-1</sup>. The VLA spectral line system also provided a continuum channel, which recorded the average power of the central 75% of the total available bandpass. The array was in the C configuration, which provided a maximum resolution of 0''.6 and made the observations insensitive to structures larger than 25'' at 22 GHz. The phase center of

the array was set at  $\alpha(1950) = 18^{\text{h}}24^{\text{m}}50\overset{\text{s}}{.}9$  and  $\delta(1950) = -11^{\circ}58'26\overset{\text{s}}{.}0$ . More details of these observations are given by GRM.

Owing to the recent improvements in imaging techniques for radio interferometric data, we decided to reprocess these data in order to obtain a better dynamic range than that achieved by GRM. The data were edited and calibrated by applying the complex gain solution from the calibration source, following the standard VLA procedures. The continuum channel was self-calibrated in phase (Schwab 1980) using the Astronomical Image Processing System (AIPS) task CALIB, and the phase corrections were applied to all spectral line channels. Maps were made with naturally weighted ( $u, v$ ) data with a Gaussian taper of 60 k $\lambda$ , which resulted in a synthesized half-power beamwidth (HPBW) of 3''.6 × 3''.1. The rms noise level in a single spectral line channel was  $\sim 6$  mJy per beam solid angle.

### 2.2. NH<sub>3</sub>(2, 2) Line

The ( $J, K$ ) = (2, 2) inversion transition of ammonia, at the rest frequency of 23,722.633 MHz, was observed with a bandpass of 6.25 MHz, centered at an LSR velocity of 50.0 km s<sup>-1</sup> with 63 spectral channels spaced at intervals of 97.625 kHz (1.2 km s<sup>-1</sup> velocity resolution). The array was in the D configuration, which provided a range of spacings from 35 to 1030 m. This range of spacings made structures larger than about 60'' undetectable. The phase center of the array was set at  $\alpha(1950) = 18^{\text{h}}24^{\text{m}}50\overset{\text{s}}{.}2$  and  $\delta(1950) = -11^{\circ}58'30\overset{\text{s}}{.}0$ .

The integration time on source was  $\sim 150$  minutes with 25 antennas. Each 15 minute on-source scan was paired with a 3 minute calibration scan on 1730–130. The data were edited and calibrated by applying the complex gain solution from the calibration source. The flux density scale was determined from an observation of 3C 286, for which we assumed a flux density of 2.4 Jy at 1.3 cm. The bandpass response was normalized using the observations of the calibrator source 1226+023. The spectral data were further calibrated by applying the solution obtained from a self-calibration procedure on the continuum channel. The uniformly weighted ( $u, v$ ) data were Fourier transformed and cleaned with the MX algorithm. The synthesized beam was 3''.4 × 2''.4. In order to improve the sensitivity to low surface brightness emission, we also made maps with a Gaussian taper of 40 k $\lambda$ , which resulted in a synthesized beam of 6''.0 × 5''.0. Line maps were made from the individual channel maps by subtracting a continuum map made from the average of all line-free channel maps. The rms noise levels in each line map were 7.1 and 5.6 mJy per beam solid angle for the uniform and tapered line maps, respectively.

<sup>4</sup> The National Radio Astronomy Observatory is operated by Associated Universities, Inc., under cooperative agreement with the National Science Foundation.

TABLE 2  
OBSERVED RADIO CONTINUUM PARAMETERS

| H II REGION | POSITION        |                 | FREQUENCY<br>(GHz) | FLUX DENSITY<br>(Jy) | ANGULAR SIZE<br>(arcsec) |
|-------------|-----------------|-----------------|--------------------|----------------------|--------------------------|
|             | $\alpha$ (1950) | $\delta$ (1950) |                    |                      |                          |
| A .....     | 18 24 50.35     | -11 58 34.2     | 1.6                | 0.40                 | ...                      |
|             |                 |                 | 4.9                | 1.37                 | 3.4                      |
|             |                 |                 | 22.4               | 0.93                 | 3.1                      |
| B .....     | 18 24 49.55     | -11 58 26.5     | 1.6                | 0.22                 | 5.3                      |
|             |                 |                 | 4.9                | 0.53                 | 2.1                      |
|             |                 |                 | 22.4               | 0.26                 | 1.5                      |
| CD .....    | 18 24 50.36     | -11 58 25.9     | 1.6                | 1.15                 | 10.8                     |
|             |                 |                 | 4.9                | 2.65                 | 10.1                     |
|             |                 |                 | 22.4               | 1.41                 | 8.9                      |
| E .....     | 18 24 50.94     | -11 58 39.3     | 1.6                | 0.63                 | 13.0 <sup>a</sup>        |
|             |                 |                 | 4.9                | 0.89                 | ...                      |
|             |                 |                 | 22.4               | 0.42                 | ...                      |
| F .....     | 18 24 50.22     | -11 58 30.0     | 1.6                | 0.056                | ...                      |
|             |                 |                 | 4.9                | 0.12                 | 1.5                      |
|             |                 |                 | 22.4               | 0.13                 | 1.8                      |

NOTE.—Units of right ascension are hours, minutes, and seconds, and units of declination are degrees, arcminutes, and arcseconds.

<sup>a</sup> Outer shell radius.

### 2.3. Continuum Observations

Continuum observations were made at 1.6275 GHz with the array in the A configuration, which provided a range of baseline spacings from 0.7 to 36 km. Hence, the observations were insensitive to structures larger than 40''. We used a bandwidth of 50 MHz and a total integration time on source of 5 minutes. Maps were made by Fourier transforming the ( $u$ ,  $v$ ) data, using uniform weighting, and cleaned using the MX algorithm. The resulting synthesized HPBW was 1''.5  $\times$  1''.2 and the rms noise level was 0.31 mJy beam<sup>-1</sup>. Continuum measurements were also available at 22.4 GHz from the continuum channel of the H66 $\alpha$  observations (the average of the central 75% of the 12.5 MHz bandpass). In addition, a 4.9 GHz map was made from the VLA data (epoch 1979) described in Ho & Haschick (1981), which was provided to us by P. T. P. Ho (private communication). These data could not be calibrated in amplitude with respect to a standard VLA amplitude calibrator, and therefore it is possible that the flux densities at this frequency could have significant systematic errors.

## 3. RESULTS

### 3.1. Radio Continuum Maps

Maps of the radio continuum emission from the G19.6-0.2 star-forming region, at the frequencies of 1.6, 4.9, and 22.4 GHz, are presented in Figure 1. These maps illustrate the complex appearance of this region. We identify a bright and compact cometary-like component located near the center of the maps (object A), two extended components, one lying toward the north (object CD) and the other toward the southeast (object E) of the bright source, and a relatively compact component (object B) located  $\sim$  14'' to the northwest of source A. The letters labeling the components follow the notation of Ho & Haschick (1981), who identified five emission components at 4.9 GHz. The overall morphology obtained by Ho & Haschick is in good agreement with that observed by us.

The morphology of the individual components can be seen more clearly in the gray-scale image of the 1.6 GHz radio continuum emission shown in Figure 2. Object A appears to have a broken-shell or cometary morphology,

exhibiting a bright western hemisphere. Component B exhibits a shell structure with a diameter of  $\sim$  6'', which is preferentially brightened on the southwestern side. The northern region (which encompasses components C and D of Ho & Haschick 1981) shows a bright, clumpy, central ridge of emission that is surrounded by a weak ring of emission with a diameter of  $\sim$  15''. Toward the diffuse component E we identify two large filaments of emission in the form of arcs with diameters of  $\sim$  20'' and 26''. The arc-shaped filaments associated with source E probably correspond to ionization fronts that separate the diffuse H II region from an extended diffuse molecular cloud. The shells could also correspond to stellar wind-blown bubbles. Table 2 lists the observed parameters of the individual components.

### 3.2. H66 $\alpha$ Line

To produce maps of line emission we subtracted a continuum map made from the average of the off-line channels from each individual channel map. Spectral maps in the velocity range from 72.1 to  $-6.5$  km s<sup>-1</sup> are shown in Figure 3. Emission in the H66 $\alpha$  line was detected from components A, B, CD, and F. Fitted Gaussian profiles and the observed spectra of the emission integrated over each of the individual H II regions are shown in Figure 4. Also shown are the spectra integrated over the whole G19.6-0.2 complex. The fitted parameters (line flux density, line-center velocity, and line width) and the line-to-continuum flux-density ratios are given in Table 3.

The systemic velocity of the ionized gas in G19.6-0.2, defined as the mean velocity of the composite spectra, is

TABLE 3  
H66 $\alpha$  LINE PARAMETERS

| H II Region | $S_L$<br>(Jy) | Velocity<br>(km s <sup>-1</sup> ) | Line Width<br>(km s <sup>-1</sup> ) | $S_L/S_C$ |
|-------------|---------------|-----------------------------------|-------------------------------------|-----------|
| A .....     | 0.260         | $36.9 \pm 1.4$                    | $28.2 \pm 1.1$                      | 0.29      |
| B .....     | 0.075         | $43.0 \pm 1.5$                    | $30.1 \pm 4.0$                      | 0.31      |
| CD .....    | 0.420         | $44.3 \pm 0.4$                    | $25.5 \pm 1.1$                      | 0.35      |
| F .....     | 0.046         | $42.2 \pm 1.0$                    | $27.8 \pm 2.6$                      | 0.29      |
| Whole ..... | 0.740         | $41.5 \pm 0.4$                    | $27.3 \pm 1.0$                      | ...       |

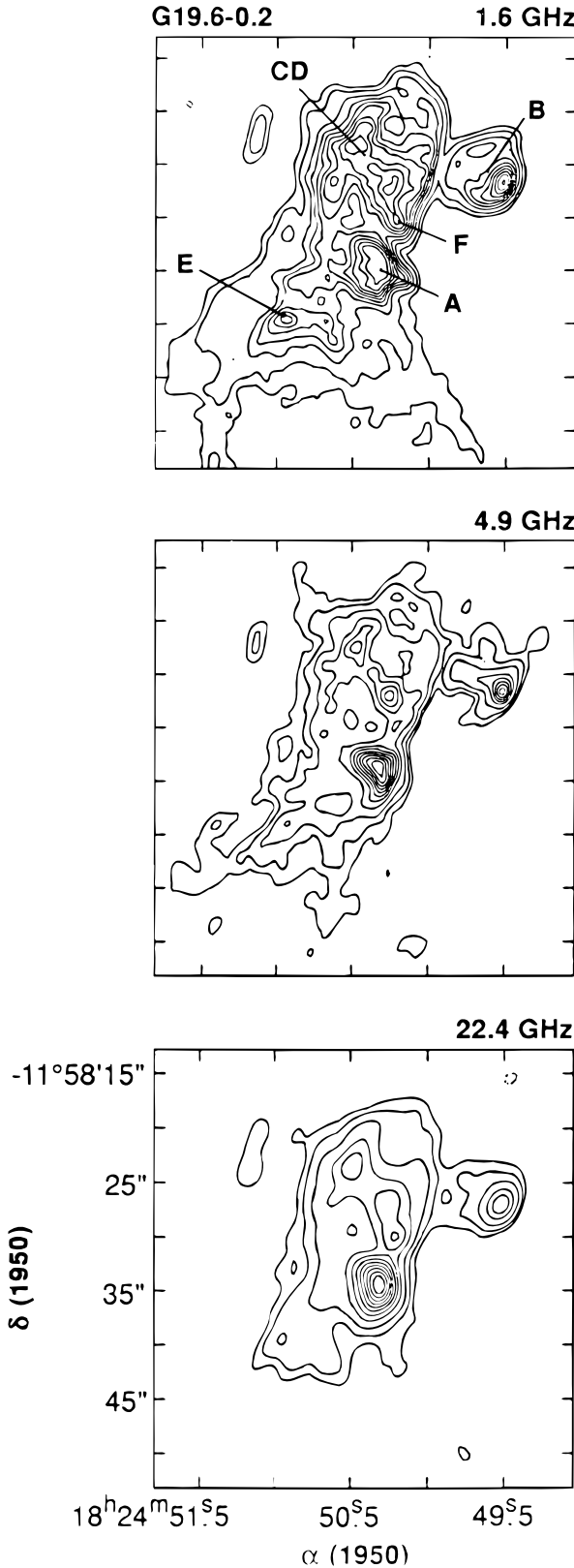


FIG. 1.—VLA radio continuum maps toward G19.6–0.2. *Top panel:* 1.6 GHz map. Contour levels are  $-5, 5, 10, 20, 30, 40, 50, 60, 70, 80$ , and 90 percent of the peak brightness of  $28.1 \text{ mJy beam}^{-1}$ . The angular resolution is  $1''.5 \times 1''.2$ . *Middle panel:* 4.9 GHz map. Contour levels are  $-2.5, 2.5, 5, 10, 20, 30, 40, 50, 60, 70, 80$ , and 90 percent of the peak brightness of  $206 \text{ mJy beam}^{-1}$ . The angular resolution is  $1''.6 \times 1''.2$ . *Bottom panel:* 22.4 GHz map. Contour levels are  $-2.5, 2.5, 5, 10, 20, 30, 40, 50, 60, 70, 80$ , and 90 percent of the peak brightness of  $309 \text{ mJy beam}^{-1}$ . The angular resolution is  $2''.5 \times 1''.9$ .

$41.5 \pm 0.4 \text{ km s}^{-1}$ . However, the central velocities of the H66 $\alpha$  line emission derived from the individual components are distinctly different. The central velocity of component A is shifted by  $-4.6 \text{ km s}^{-1}$  with respect to the average velocity of the whole complex, while that of component CD is shifted by  $2.8 \text{ km s}^{-1}$ . Emission from the shell-like source B was detected only from its brighter edge, with a shift of  $1.5 \text{ km s}^{-1}$ . We also find that there is a velocity gradient across component A from roughly southwest to northeast, with the most blueshifted velocities in the southwest. The magnitude of the velocity shift is  $\sim 5 \text{ km s}^{-1}$  across an angular distance of  $\sim 4''$ .

### 3.3. NH<sub>3</sub>(2, 2) Line

Spectral maps of the ammonia emission in the (2, 2) transition were made from the individual channel maps and corrected for continuum emission by subtraction of a continuum map made from the average of all line-free channel maps. Line maps in the velocity range from  $71.0$  to  $19.1 \text{ km s}^{-1}$  are presented in Figure 5. Each panel in this figure shows the average of the emission from three consecutive individual line maps (effective velocity width of  $3.7 \text{ km s}^{-1}$ ). The center velocity of each map is shown in the top right-hand corner. The central line maps (velocities from  $45.1$  to  $34.0 \text{ km s}^{-1}$ ), which cover the range of velocities of the main hyperfine (HF) line, exhibit three distinct features: a bright component located near the center of the map; an absorption component located toward the north of the bright feature (see the  $45.1 \text{ km s}^{-1}$  channel); and a weak elongated emission feature located toward the southwest of the bright feature (see the  $41.4 \text{ km s}^{-1}$  channel). The outer line maps, which sample the emission from the satellite HF lines ( $1 \rightarrow 2$ :  $67.3$  and  $63.6 \text{ km s}^{-1}$  channels;  $3 \rightarrow 2$ :  $59.9$  and  $56.2 \text{ km s}^{-1}$  channels;  $2 \rightarrow 3$ :  $26.6$  and  $22.8 \text{ km s}^{-1}$  channels), show that the satellite emission arises only from the central component. The observed parameters of the ammonia structures are summarized in Table 4.

The overall morphology of the ammonia emission from the high-density molecular gas toward the G19.6–0.2 region can be seen in the upper panel of Figure 6, which shows the zeroth moment (flux density integrated over the velocity range of  $30.3$  to  $47.5 \text{ km s}^{-1}$ ) distribution of the emission in the main HF line. The observed brightness distribution can be roughly characterized as arising from three structures: (1) a central optically thick clump, with an angular size of  $3''.7 \times 2''.6$  (hereafter referred to as the middle clump); (2) an elongated ( $8''.4 \times 3''.0$ ) optically thin structure toward the southwest (hereafter, the southwestern clump); and (3) an optically thin clump seen in absorption toward the north (hereafter, the northern clump). The morphology of the densest region of the middle clump is shown in the lower panel of Figure 6, a map of the average emission in the three HF satellite lines of the (2, 2) inversion transition within our spectral range (HF lines  $1 \rightarrow 2$ ,  $3 \rightarrow 2$ , and  $2 \rightarrow 3$ ). From this map we measured FWHM angular diameters for the denser molecular gas within the middle clump of  $3''.5 \times 1''.5$  at P.A.  $160^\circ$ . Also plotted in the lower panel are the positions of the OH maser spots toward G19.6–0.2, taken from GRM.

The (2, 2) inversion transition spectra, integrated over the angular extent of each ammonia clump, are shown in Figure 7. Emission from the middle clump was detected in the main and the three satellite HF lines within the observed velocity range (the  $2 \rightarrow 1$  satellite line falls outside the observed

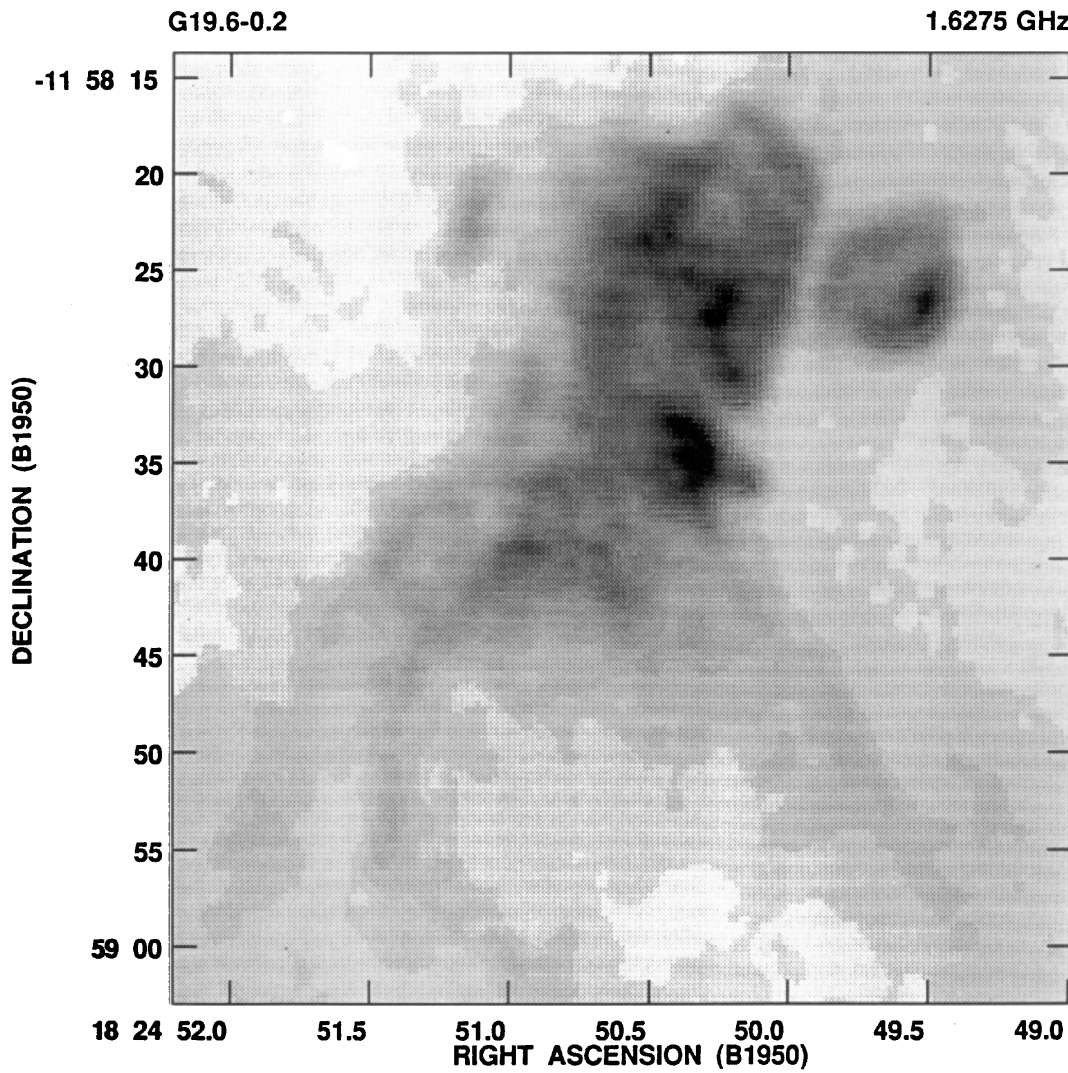


FIG. 2.—Gray-scale map of the radio continuum emission at 1.6 GHz from G19.6-0.2. Gray scale ranges from  $-1.5$  to  $28.1$  mJy beam $^{-1}$ . The angular resolution is  $1''.5 \times 1''.2$ .

bandwidth). The strong intensity of the satellite lines (at  $+25.8$ ,  $+16.6$ , and  $-16.6$  km s $^{-1}$  from the main line) indicates that they have significant optical depths. The average radial velocity of the ammonia emission from the middle clump, determined by simultaneously fitting Gaussian profiles to the three satellite HF lines with fixed velocity separations, was  $40.4 \pm 0.9$  km s $^{-1}$ . The average line width of the emission in the satellite lines was  $6.7 \pm 0.5$  km s $^{-1}$ . Toward the northern clump we detected the (2, 2) main line in absorption. The line-center velocity and line width of the absorption feature were  $45.1$  and  $4.2$  km s $^{-1}$ , respectively. The satellite lines were below our detection limits. The

upper limit ( $3\sigma$ ) for the flux density per beam in the satellite lines was  $10.8$  mJy in a  $3''.4 \times 2''.4$  beam. Toward the southwestern clump the (2, 2) main line was detected in emission with a line-center velocity of  $41.8$  km s $^{-1}$  and a line width of  $5.5$  km s $^{-1}$ .

Figure 8 shows velocity-position contour diagrams of the emission in the (2, 2) inversion transition, made from cuts along the directions marked by solid lines in Figure 6. In the upper diagram, made from a cut of the untapered maps along a direction with a position angle of  $0^\circ$  and  $\alpha = 18^{\mathrm{h}}24^{\mathrm{m}}50^{\mathrm{s}}.28$ , the most prominent feature is a broad velocity component ( $\sim 7$  km s $^{-1}$  wide) located roughly at  $\sim 1''$  offset

TABLE 4  
OBSERVED PARAMETERS OF AMMONIA CLOUDS

| CLUMP          | POSITION        |                 | HF LINE                                | FLUX DENSITY<br>(mJy)     | VELOCITY<br>(km s $^{-1}$ )      | LINE WIDTH<br>(km s $^{-1}$ )  | ANGLE SIZE<br>(arcsec)                       | P.A.<br>(deg.) |
|----------------|-----------------|-----------------|--|---------------------------|----------------------------------|--------------------------------|--|----------------|
|                | $\alpha$ (1950) | $\delta$ (1950) |  |                           |                                  |                                |  |                |
| Middle .....   | 18 24 50.26     | -11 58 31.5     | (2, 2; <i>m</i> )<br>(2, 2; <i>s</i> ) | $197 \pm 6$<br>$91 \pm 7$ | $39.3 \pm 0.1$<br>$40.4 \pm 0.9$ | $9.5 \pm 0.3$<br>$6.6 \pm 0.8$ | $3''.7 \times 2''.6$<br>$0''.0 \times 0''.0$ | 81<br>...      |
| North .....    | 18 24 50.33     | -11 58 24.5     | (2, 2; <i>m</i> )                      | $-74 \pm 5$               | $45.1 \pm 0.1$                   | $4.2 \pm 0.3$                  | $\leq 2''.7$                                 | ...            |
| Southwest..... | 18 24 49.71     | -11 58 36.1     | (2, 2; <i>m</i> )                      | $74 \pm 6$                | $41.8 \pm 0.2$                   | $5.5 \pm 0.5$                  | $8''.4 \times 3''.0$                         | 32             |

NOTE.—Units of right ascension are hours, minutes, and seconds, and units of declination are degrees, arcminutes, and arcseconds.

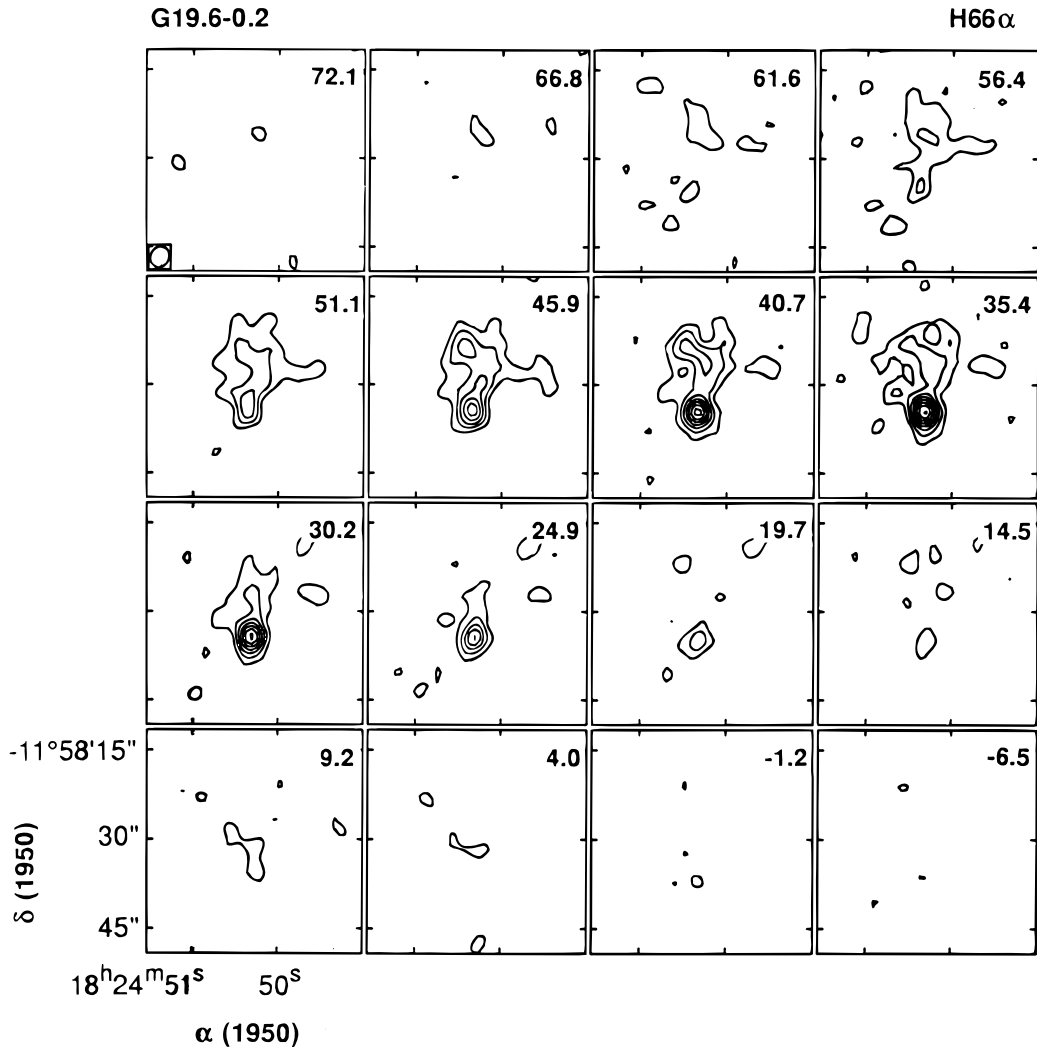


FIG. 3.—Line maps of the H66 $\alpha$  emission from G19.6–0.2. The LSR velocity, in km s $^{-1}$ , is indicated at the top right-hand corner of each line map. Contour levels are  $\{-1, 1, 2, 3, 4, 5, 6, 7, \text{ and } 8\} \times 20$  mJy beam $^{-1}$ . The (1  $\sigma$ ) rms noise in the line maps is 5.9 mJy beam $^{-1}$ . The angular resolution is 3. $'$ 6  $\times$  3. $'$ 1.

( $\delta \sim -11^{\circ}58'31''$ ) and  $v \sim 40$  km s $^{-1}$  (the middle clump). The emission in the 1  $\rightarrow$  2, 3  $\rightarrow$  2, and 2  $\rightarrow$  3 HF satellite lines from the clump can be recognized easily at the velocities of  $\sim 24$ , 57, and 66 km s $^{-1}$ , respectively. Indicated near the bottom are the expected locations of the main and satellite HF lines for a cloud with a velocity of 40.4 km s $^{-1}$ . The absorption feature (northern clump) is also clearly distinguished, at the velocity of  $\sim 45$  km s $^{-1}$  and offset of  $\sim 5.3''$  ( $\delta \sim -11^{\circ}58'26.7''$ ). In addition, in the upper diagram we identified a third kinematical feature that is spatially coincident with the middle clump but has velocities that are blueshifted with respect to the systemic velocity of the middle clump. This feature, which covers the velocity range from  $\sim 29$  to 35 km s $^{-1}$ , was detected only in the main HF transition. The lower diagram, made from a cut of the 40 k $\lambda$  maps along a direction with a position angle of 45° passing through  $\alpha = 18^{\text{h}}24^{\text{m}}50^{\text{s}}$ ,  $\delta = -11^{\circ}58'29.7''$ , clearly shows the northern clump in absorption, at a velocity of  $\sim 45$  km s $^{-1}$ , and the southwestern clump, at a velocity of  $\sim 41$  km s $^{-1}$ . Both of these features have velocity widths that are appreciably narrower than that of the middle clump, and both are only seen in the main HF line. The lack of detectable emission in the HF satellite lines suggests that these

features have considerably lower opacities than that of the middle clump. The emission seen near the center of the lower diagram corresponds to emission from the northwest edge of the middle clump.

#### 4. DISCUSSION

##### 4.1. Ionized Gas

###### 4.1.1. Cluster of H II Regions

The complex appearance of the G19.6–0.2 region of ionized gas is typical of galactic H II regions. The observed multiple structure could be due to a cluster of OB exciting stars, the presence of density inhomogeneities within an extended H II region excited by a single luminous star, or a combination of both. On the basis of the radio continuum morphology, the distinction between a density clump and an actual compact H II region is difficult to make. Ho & Haschick (1981) interpreted the overall morphology of G19.6–0.2 in terms of excitation by several sources. They modeled the brightness distribution with five distinct spherical components: two bright and relatively compact objects (components A and B), and three more extended and weaker sources (components C, D, and E). As discussed in

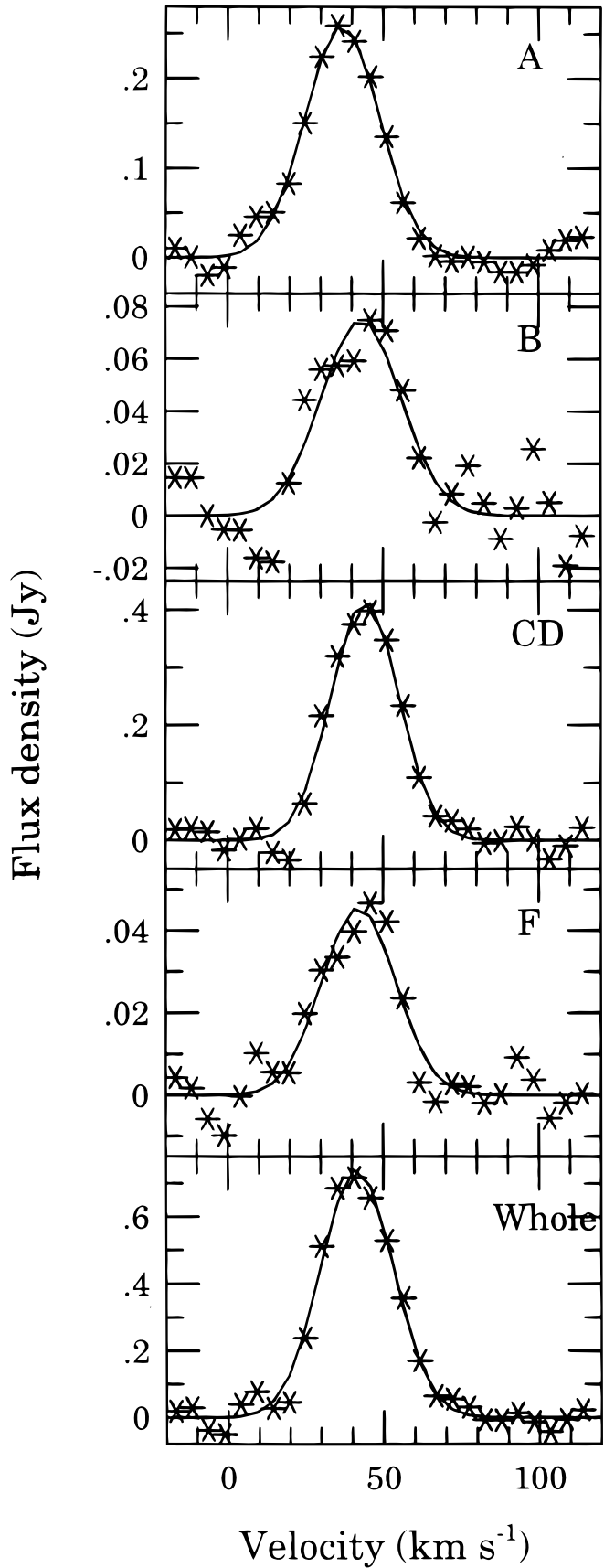


FIG. 4.—Profiles of integrated H $66\alpha$  line emission from each individual H II region and from the whole ionized complex.

§ 3.1, our map of the radio continuum emission at 1.6 GHz (see Fig. 2), which is more sensitive to lower surface brightness emission, reveals complex morphological features within each of the individual components, showing that the H II components cannot be well represented by spherical distributions. Among the most striking features are the presence of shell-like and arclike structures. From the radio continuum observations we identify four distinct ionized structures, with sizes ranging from 0.1 to 0.4 pc, which have shell-like and arclike morphologies. Toward the center of the G19.6-0.2 region, GRM reported a compact source located close to the center of OH maser emission. Our observations show that this source (hereafter component F) has an angular size of  $\sim 1.6''$  and peak brightness temperatures of 6200 and 3070 K at 1.6 and 4.9 GHz, respectively. It is not clear, however, whether this is a separate component or a clump within the inhomogeneous CD region.

Our continuum and recombination line observations strongly support the hypothesis, originally made by Ho & Haschick (1981), that there are several OB stars within a region of  $\sim 0.7$  pc in diameter in G19.6-0.2. The H $66\alpha$  line observations show that the distinct components have different systemic velocities, implying that they correspond to H II regions excited by different stars. The average separation between the H II components is 0.2 pc, similar to the separation of infrared objects within molecular clouds of  $\sim 0.1$  pc (Beichman, Becklin, & Wynn-Williams 1979). Based on the H $66\alpha$  observations, which show that the velocity of the ionized gas is roughly the same throughout the whole northern region, the emission from sources C and D, which show a common shell-like envelope structure, might be excited by a single star, rather than by different ones.

If the A, B, CD, E, and F sources are each ionized by single zero-age main sequence (ZAMS) stars, the rate of ionizing photons needed to excite them (see Table 5) indicates stars with spectral types of O8.5, O9.5, O7.5, O9, and B0, respectively. The total luminosity emitted by this cluster of O and B stars, as inferred from the radio observations (see Table 5), is  $2.3 \times 10^5 L_\odot$ . This value is consistent with the luminosity of the whole region in the far infrared (1–1300  $\mu$ m wavelength) range of  $1.6 \times 10^5 L_\odot$  (Chini, Krügel, & Wargau 1987; value corrected to the adopted distance of 3.5 kpc). We cannot rule out the possibility that more than one star might be responsible for the ionization of each of the individual H II regions. In this case the spectral type of the most luminous star within the cluster will be of a later type than that derived from the single-star hypothesis.

#### 4.1.2. Physical Parameters

The electron temperatures of the H II regions can be estimated from the H $66\alpha$  recombination line data. If the ionized gas is in local thermodynamic equilibrium (LTE), the electron temperature  $T_e^*$  is given by:

$$T_e^* = 2.21 \times 10^3 \left( \frac{v}{\text{GHz}} \right)^{0.96} \left( \frac{S_L}{S_C} \right)^{-0.87} \times \left( \frac{\Delta v}{\text{km s}^{-1}} \right)^{-0.87} (1 + y^+)^{-0.87} \text{ K},$$

where  $S_L/S_C$  is the line-to-continuum ratio of flux densities,  $\Delta v$  is the observed line width (FWHM),  $v$  is the frequency of the line, and  $y^+$  is the single ionized helium-to-ionized

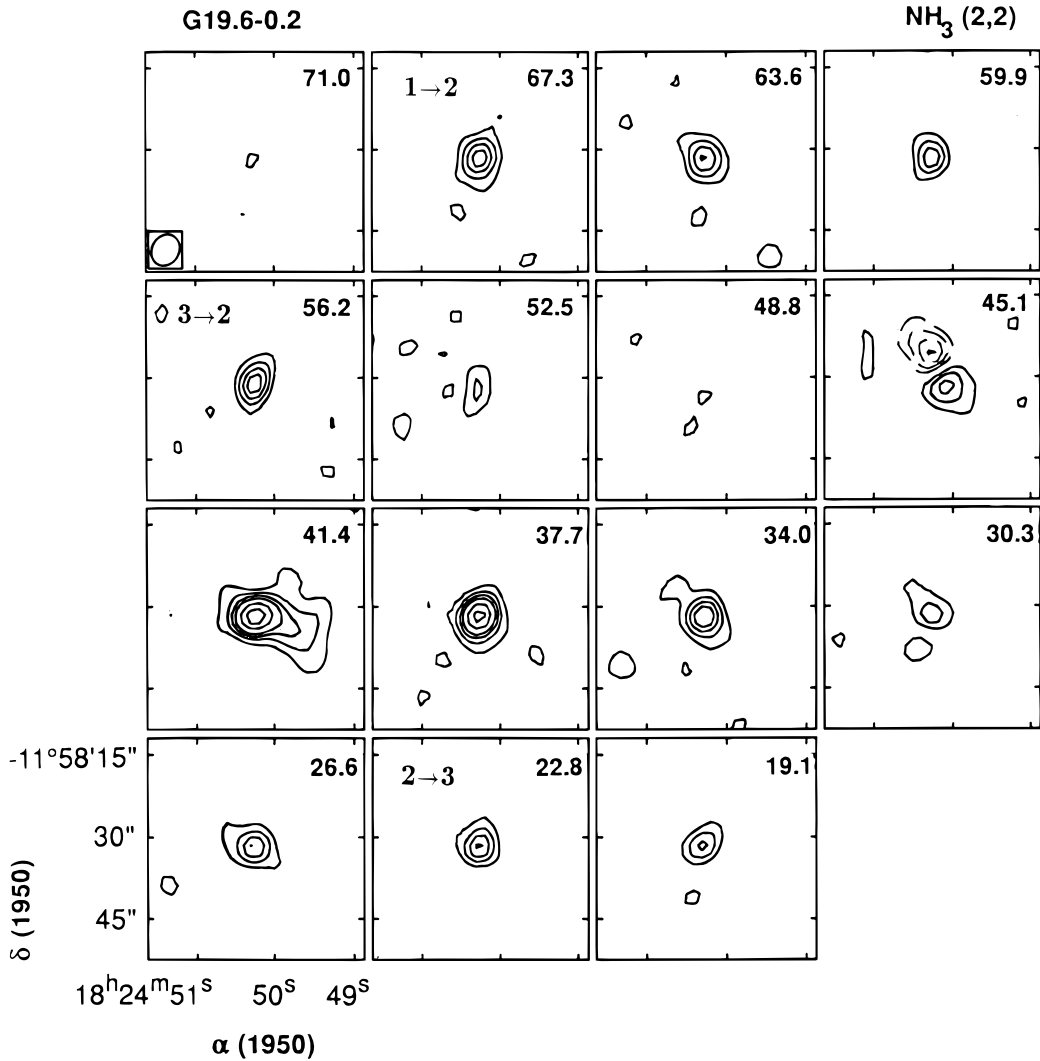


FIG. 5.—Line channel maps of the emission in the (2, 2) inversion transition of ammonia toward G19.6–0.2 with  $6.^{\circ}0 \times 5.^{\circ}0$  angular resolution. The LSR central velocity of each map is indicated at the top right-hand side of each map. The locations of the satellite hyperfine components, with the assumption of an LSR velocity of  $40.4 \text{ km s}^{-1}$  for the main hyperfine component (see text), are indicated at the top of the appropriate panels by their  $F' \rightarrow F$  values. Contour levels are  $\{-4, -3, -2, -1, 1, 2, 3, 4, 6, \text{ and } 8\} \times 13 \text{ mJy beam}^{-1}$ . Negative contour levels are represented by dashed lines. The  $(1\sigma)$  rms noise in the line maps is  $5.6 \text{ mJy beam}^{-1}$ .

hydrogen number ratio. The LTE temperatures are given in column (2) of Table 5. Owing to the effects of stimulated emission, which produces an enhancement of the line emission and consequently of the line-to-continuum ratio (see Brown, Lockman, & Knapp 1978), the LTE temperatures may not be reliable estimates of the true electron temperatures. In order to assess the importance of stimulated emission in the H $66\alpha$  line for the H II regions studied here, we computed non-LTE models for the line-to-continuum ratio. Using an iterative procedure to fit simultaneously the

observed line-to-continuum ratio, radio continuum spectra, and line width (see Garay, Lizano, & Gómez 1994 for a description of the method), we derive the electron temperatures given in column (3) of Table 5. The  $T_e/T_e^*$  ratios range from 1.14 to 1.25, showing that the LTE temperatures underestimate the actual electron temperatures by  $\sim 20\%$ . Two parameters derived from this procedure, which assumes that the sources can be modeled as homogeneous, constant-density regions of ionized gas, are the solid angle of the source,  $\Omega_{\text{BB}}$ , and the emission measure through the

TABLE 5  
DERIVED PARAMETERS OF H II REGIONS<sup>a</sup>

| H II Region<br>(1) | $T_e^*$<br>(K)<br>(2) | $T_e$<br>(K)<br>(3) | $\Omega_{\text{BB}}$<br>(arcsec $^2$ )<br>(4) | $EM$<br>(pc cm $^{-6}$ )<br>(5) | $N_e$<br>(cm $^{-3}$ )<br>(6) | $N_i$<br>(s $^{-1}$ )<br>(7) | Spectral Type<br>(ZAMS)<br>(8) | $\mathcal{L}$<br>( $L_\odot$ )<br>(9) |
|--------------------|-----------------------|---------------------|---|---------------------------------|-------------------------------|------------------------------|--------------------------------|---------------------------------------|
| A .....            | 6400                  | 8000                | 22.0  | $2.8 \times 10^7$               | $1.8 \times 10^{48}$          | $1.6 \times 10^{48}$         | O8.5                           | $5.3 \times 10^4$                     |
| B .....            | 5700                  | 6500                | 22.0  | $8.6 \times 10^6$               | $9.9 \times 10^3$             | $5.9 \times 10^{47}$         | O9.5                           | $3.6 \times 10^4$                     |
| CD .....           | 6050                  | 6900                | 109.0   | $8.7 \times 10^6$               | $6.7 \times 10^3$             | $2.8 \times 10^{48}$         | O7.5                           | $7.5 \times 10^4$                     |
| E .....            | ...                   | 7000                | 82.0  | $4.0 \times 10^6$               | $4.9 \times 10^3$             | $9.7 \times 10^{47}$         | O9                             | $4.3 \times 10^4$                     |
| F .....            | 6550                  | 7500                | 3.7   | $1.8 \times 10^7$               | $2.2 \times 10^4$             | $1.9 \times 10^{47}$         | B0                             | $2.4 \times 10^4$                     |

<sup>a</sup> Based on a distance of 3.5 kpc.

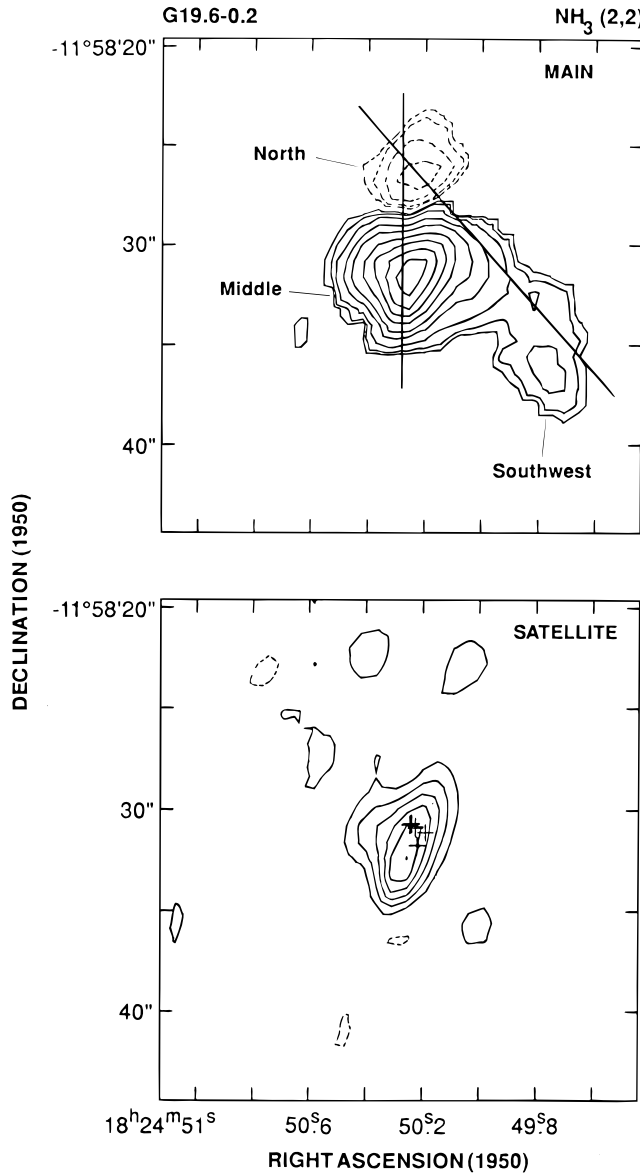


FIG. 6.—*Top panel:* Map of the zero-order moment (velocity-integrated flux density) of the emission in the  $\text{NH}_3(2, 2)$  main hyperfine line from G19.6–0.2. The range of velocity integration is  $30.3$ – $47.5 \text{ km s}^{-1}$ . The angular resolution is  $3.^{\circ}4 \times 2.^{\circ}4$ . *Bottom panel:* Map of the average satellite line emission from G19.6–0.2. Contour levels are  $\{-1, 1, 2, 3, 4, 5, 6\} \times 7 \text{ mJy beam}^{-1}$ . The angular resolution is  $3.^{\circ}4 \times 2.^{\circ}4$ . The plus signs mark the positions of the OH masers.

center of the source,  $EM$ . These parameters are given in columns (4) and (5) of Table 5. The electron densities given in column (6) of Table 5 were computed from the emission measures by use of the relation  $N_e = [EM/(1 + y^+)]L]^{1/2}$ , where  $L$  is the path length along the line of sight, estimated as  $L = (\Omega_{\text{BB}})^{1/2}D$ , and  $D$  is the distance to the source, assumed to be 3.5 kpc (CWC). The number of ionizing photons needed to excite each of the H II regions,  $N_i$ , is given in column (7) of Table 5.

#### 4.1.3. Density Inhomogeneities

Most of the individual H II regions discussed above are probably not homogeneous in density. In a survey of radio continuum emission from massive-star-forming regions, made with high angular resolution ( $0.^{\circ}4$ ), Wood & Churchwell (1989; hereafter WC) detected several ultracompact (UC) irregular regions of ionized gas toward G19.6–0.2, all

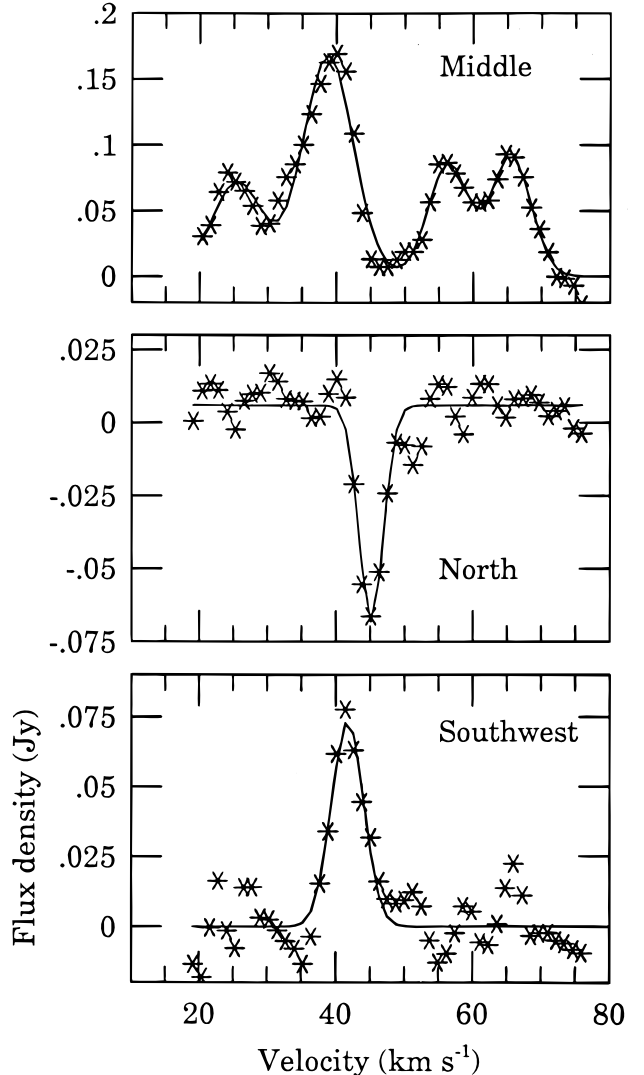


FIG. 7.—Spectra of the  $\text{NH}_3(2, 2)$  line emission integrated over each individual ammonia cloud.

of which were found projected within the larger, but still compact, H II regions. Toward the northern region, WC completely resolved the extended emission and detected a few multiple-peaked irregular condensations. A notable characteristic of the condensations detected by WC is that, even though they are very compact, their brightness temperatures are not significantly different from those of the more extended associated H II regions. For example, toward the H II region B, WC detected an elongated ultracompact object with a flux density at 14.9 GHz of 32 mJy, a peak brightness temperature of 400 K, and an angular size of  $\sim 1.^{\circ}1 \times 0.^{\circ}3$ . Its location coincides with the brightest edge of the shell structure seen with lower angular resolution (see Fig. 1a). For source B we measured a flux density at 4.9 GHz of 530 mJy and a peak brightness of 5800 K. If we assume that this emission is optically thin thermal radiation, then its expected brightness temperature at 14.9 GHz is  $\sim 550$  K, similar to the value observed for the associated UC condensation.

There are several possible sources of excitation for the multiple peaks found within the extended H II regions. If the compact structures are externally ionized, then they would correspond to density inhomogeneities within the larger region of ionized gas excited by a single star, while if they

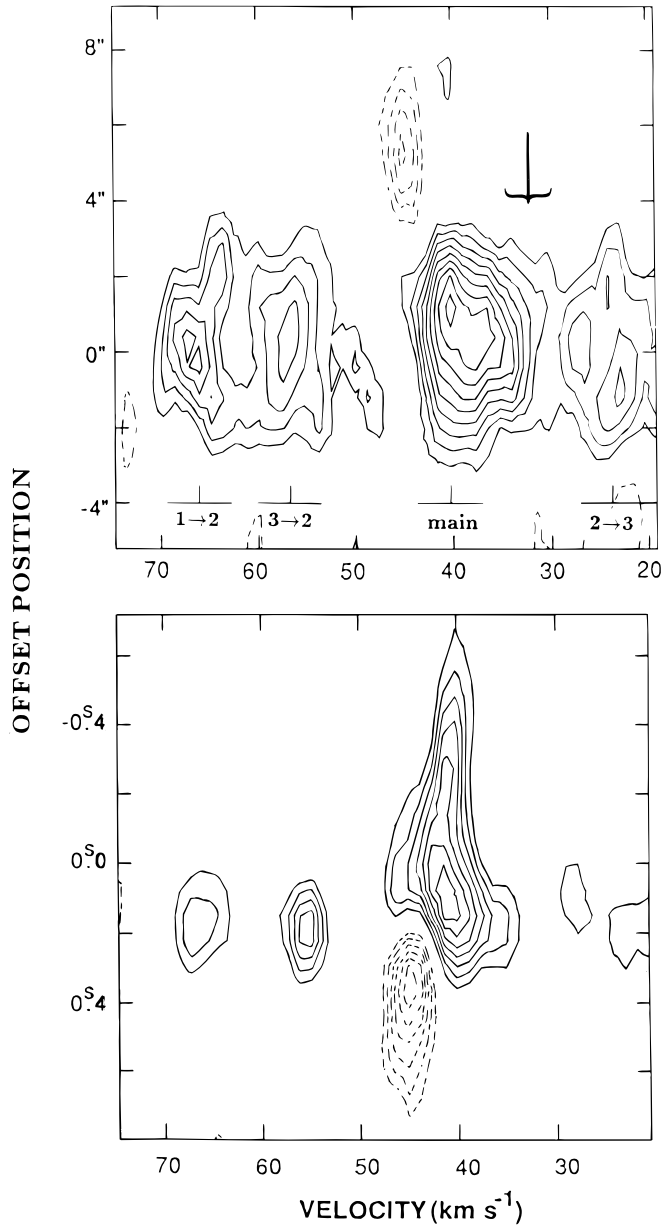


FIG. 8.—Position-velocity diagrams of the (2, 2) ammonia line emission and absorption from G19.6–0.2. *Top Panel:* Diagram along a direction with P.A. of  $0^\circ$  passing through  $\alpha = 18^{\text{h}}24^{\text{m}}50\overset{\text{s}}{.}28$ , (see Fig. 6). Offsets, in arcseconds, are relative to  $\delta = -11^\circ58'32''$ . Contour levels are  $(-5, -4, -3, -2, 2, 3, 4, 5, 6, 7, 8, 9, \text{ and } 10) \times 7 \text{ mJy beam}^{-1}$ . The angular resolution is  $3''.4 \times 2''.4$ . The expected location of the main and satellite HF lines for a cloud with a rest velocity of  $40.4 \text{ km s}^{-1}$  and a line width of  $6.6 \text{ km s}^{-1}$  are indicated at the bottom of the panel. *Bottom Panel:* Diagram along a direction with P.A. of  $45^\circ$  passing through  $\alpha = 18^{\text{h}}24^{\text{m}}50\overset{\text{s}}{.}00$ ,  $\delta = -11^\circ58'29''$ . Offsets, in seconds of time, are relative to this position. Contour levels are  $\{-5, -4, -3, -2, 2, 3, 4, \text{ and } 5\} \times 7 \text{ mJy beam}^{-1}$ . The angular resolution is  $6''.0 \times 5''.0$ .

are internally ionized, they would harbor an energy source of their own. We first consider the latter hypothesis. For classical (i.e., internally excited) H II regions, the electron density  $N_e$  and diameter  $L$  are found to be highly correlated (see Habing & Israel 1979). From the condition of ionization equilibrium it is expected that  $N_e \propto \overline{N}_i^{1/2} L^{-3/2}$ , where  $\overline{N}_i$  is an average number of ionizing photons, and hence that the emission measure ( $EM \propto N_e^2 L$ ) should vary as  $\overline{N}_i L^{-2}$ . Thus, we expect ultracompact H II regions to have considerably larger emission measures and hence greater brightness,

since  $T_b \propto EM$ , than the more extended H II regions. This expectation is not met for the ultracompact objects in G19.6–0.2 because they show similar brightness temperatures to those of the associated extended H II regions. This argues against the internal-excitation hypothesis. We suggest that the emission from the ultracompact objects most likely corresponds to optically thin thermal radiation arising from the denser structures embedded within a less compact inhomogeneous region of ionized gas. The similar brightness exhibited by the ultracompact and larger regions of ionized gas is readily explained, because the number of ionizing photons exciting the ultracompact regions is considerably smaller than the number of UV photons emitted by the exciting star.

High angular resolution radio continuum surveys of our Galaxy have shown the presence of a large number of ultracompact H II regions with characteristics similar to those found in G19.6–0.2 (WC; Kurtz, Churchwell, & Wood 1994). On the assumption that the ages of these compact H II regions correspond to their dynamical ages, their small sizes would imply that they are very young objects. The large number of ultracompact H II regions and their short dynamical ages pose the well-known problem that the rate of massive-star formation appears to be much greater than other indicators suggest (WC, Churchwell 1990). Many of the ultracompact ionized sources observed in G19.6–02 and in other star-forming regions may not be excited by embedded stars, but may be manifestations of density inhomogeneities within larger H II regions that are excited by a single luminous star. In this picture, the ultracompact structures are externally ionized. If completely ionized, the clumps must exist close to the edge of the H II region and may exhibit the clumpy structure of the neutral material into which the H II region is expanding. Alternatively, the clumps may be partially ionized dense globules within the H II region produced by the fragmentation of the accreting molecular gas that collapsed to form the central exciting star. Lizano et al. (1996) have shown that the clumpy structure of the ambient medium can result in long-lived compact H II regions, naturally explaining the apparent discrepancy between the large number of compact H II regions and their short dynamical ages.

#### 4.2. Molecular Gas

In this section we derive the physical parameters of the ammonia clumps from the observations of the (2, 2) inversion transition. These parameters are summarized in Table 6.

##### 4.2.1. Middle Clump

The detection of emission in both the satellite and main HF lines of the (2, 2) inversion transition allows a direct estimate of optical depth (see Ho & Townes 1983). From the observed peak flux densities per beam in the main and satellite lines, of  $90$  and  $57 \text{ mJy beam}^{-1}$ , respectively, and the

TABLE 6  
DERIVED PARAMETERS OF AMMONIA CLUMPS

| Clump             | $T_K$<br>(K) | $\tau(2, v2)$ | $L$<br>(pc) | $N(\text{NH}_3)$<br>( $\text{cm}^{-2}$ ) | $n(\text{H}_2)$<br>( $\text{cm}^{-3}$ ) | Mass <sup>a</sup><br>( $M_\odot$ ) |
|-------------------|--------------|---------------|-------------|--|---|------------------------------------|
| Northern .....    | 30           | 0.8           | 0.046       | $6 \times 10^{15}$                       | $2 \times 10^5$                         | ...                                |
| Middle .....      | 30           | 20.0          | 0.046       | $2 \times 10^{17}$                       | $9 \times 10^6$                         | 25                                 |
| Southwestern..... | 30           | 0.3           | 0.048       | $3 \times 10^{15}$                       | $1 \times 10^5$                         | 4                                  |

<sup>a</sup> Based on an  $[\text{NH}_3/\text{H}_2]$  ratio of  $2 \times 10^{-7}$ .

assumption that these HF lines have equal beam-filling factors and excitation temperatures, we find that the opacity in the satellite line,  $\tau(2, 2; s)$ , is 1.0. The total opacity of the (2, 2) inversion transition,  $\tau(2, 2)$ , is then  $\sim 20$ .

The kinetic temperature  $T_K$  of the middle clump can be estimated from the observed peak brightness temperature  $T_b$  in the (2, 2) main line, with the assumptions that the line is optically thick, the molecular gas is in thermodynamic equilibrium, and the line emission fills the beam. The first requirement is certainly fulfilled by the (2, 2) main HF line, since toward the middle clump we derived a peak opacity of  $\sim 16$ . The second requirement is also likely to be fulfilled due to the large hydrogen molecular density,  $\sim 9 \times 10^6 \text{ cm}^{-3}$ , derived for this clump (see discussion below). The validity of the third condition can be established only with observations with higher angular resolution. Hence, only a lower limit to the kinetic temperature can be derived. From the observed peak flux density in the main line (90 mJy in a  $3''\text{4} \times 2''.\text{4}$  beam) we find  $T_b = 23 \text{ K}$ , implying  $T_K > 23 \text{ K}$ . Another estimate of the kinetic temperature of the molecular gas is provided by the temperature of the dust. From observations at 100 and 1300  $\mu\text{m}$  wavelengths, Chini et al. (1986) derived a dust temperature of 25 K for the G19.6–0.2 region. We note that this temperature is likely to correspond to an average temperature of the dust up to large distances (of order 1 pc) from the luminous stars and thus may not be appropriate for the clumps. In any case, even though we cannot establish a precise value for the kinetic temperature of the dense molecular gas toward G19.6–0.2, we conclude that there is not strong evidence for hot dust (several hundred degrees) close to the H II regions as observed in other star-forming regions (Garay & Rodríguez 1990; CWC; Olmi, Cesaroni, & Walmsley 1993). In the following calculations we will adopt a value of 30 K for the kinetic temperature of the dense molecular gas in G19.6–0.2.

Assuming that all energy levels are populated according to LTE, we can derive the total column density of ammonia,  $N(\text{NH}_3)$ , if the optical depth, line width, excitation temperature, and rotational temperature of an inversion transition are known (see eq. [8] of Garay & Rodríguez 1990). Using  $\tau(2, 2) = 20$  and  $\Delta v = 6.6 \text{ km s}^{-1}$ , and adopting excitation and rotational temperatures of 30 K, we derive a peak  $\text{NH}_3$  column density of  $2.4 \times 10^{17} \text{ cm}^{-2}$ . The ammonia density can be derived from the column density with an estimate of the characteristic length. Adopting a path length of 0.046 pc, which corresponds to the geometrical mean of the observed projected sizes, we derive an ammonia density of  $\sim 1.7 \text{ cm}^{-3}$ .

The determination of the molecular hydrogen density requires knowledge of the  $[\text{NH}_3/\text{H}_2]$  abundance ratio. For a sample of 16 molecular clouds associated with compact H II regions, Cesaroni et al. (1992) derived  $[\text{NH}_3/\text{H}_2]$  ratios in the range between  $2 \times 10^{-8}$  and  $1 \times 10^{-6}$ , with an average value of  $2 \times 10^{-7}$ . For the G19.6–0.2 molecular clump we adopt an intermediate fractional abundance of  $2 \times 10^{-7}$ . However, the ammonia abundance in clumps in the immediate neighborhood of compact H II regions may be considerably enhanced compared to more extended clouds. For example, in hot dense cores this ratio has been determined to be in the range  $10^{-6}\text{--}10^{-5}$  (Genzel et al. 1982; Mauersberger et al. 1986; Henkel, Wilson, & Mauersberger 1987). Using the adopted abundance ratio, we derive an  $\text{H}_2$  density for the molecular clump of  $9 \times 10^6 \text{ cm}^{-3}$ . This large

value is consistent with what might be expected from the close association of the clump with OH masers, which require hydrogen densities between  $10^6$  and  $10^8 \text{ cm}^{-3}$  (Reid & Moran 1981). Assuming that the clump has a spherical geometry, with a radius of 0.023 pc, we derive a molecular mass of the middle clump of  $\sim 25 M_\odot$ .

#### 4.2.2. Northern and Southwestern Clumps

The (2, 2) ammonia emission from the northern and southwestern clumps is optically thin, so the ammonia optical depths can be estimated from the observed line brightness. On the assumption that the northern absorption feature is due to the absorption of radiation from a continuum source by an optically thin ammonia medium, the line brightness in the (2, 2) main HF line,  $T_L(2, 2; m)$ , can be written as  $T_L(2, 2; m) = -T_0 X_0 \tau(2, 2; m)$ , where  $T_0$  is the beam-averaged continuum brightness temperature,  $X_0$  is the fraction of the continuum covered by the molecular gas, and  $\tau(2, 2; m)$  is the opacity of the main HF line. At the peak position of the northern clump we measured  $T_L(2, 2; m) = -12.2 \text{ K}$  and  $T_0 = 38.3 \text{ K}$ . Assuming  $X_0 = 0.5$ , a typical value derived for similar regions (e.g., W3 [OH]; Reid, Myers, & Bieging 1987), we obtain  $\tau(2, 2; m) \sim 0.6$ . Using this value of the opacity, the observed line width of  $4.2 \text{ km s}^{-1}$ , and the adopted excitation temperature,  $T_{\text{ex}} = 30 \text{ K}$ , we derive an ammonia column density of  $\sim 6 \times 10^{15} \text{ cm}^{-2}$ . For a path length of 0.046 pc (linear size corresponding to the upper limit of the angular size), we find an ammonia density of  $\sim 4 \times 10^{-2} \text{ cm}^{-3}$ . For an  $[\text{NH}_3/\text{H}_2]$  abundance ratio of  $2 \times 10^{-7}$  the molecular hydrogen density is  $\sim 2 \times 10^5 \text{ cm}^{-3}$ .

For the southwestern clump, which is not projected toward a continuum source, the line brightness can be expressed as  $T_L(2, 2; m) = T_{\text{ex}} f t(2, 2; m)$ , where  $T_{\text{ex}}$  is the excitation temperature of the line and  $f$  is the beam filling factor of the ammonia cloud. At the peak position we measured  $T_L(2, 2; m) = 8.1 \text{ K}$ , which for  $f = 1$  and  $T_{\text{ex}} = 30 \text{ K}$  implies  $\tau(2, 2; m) = 0.3$ . Using this value of the opacity and the observed line width of  $5.5 \text{ km s}^{-1}$ , we derive that the peak  $\text{NH}_3$  column density is  $\sim 3 \times 10^{15} \text{ cm}^{-2}$ . For a path length along the line of sight of 0.048 pc, corresponding to the linear size of the semiminor axis of the elongated structure, we derive an ammonia density of  $\sim 2 \times 10^{-2} \text{ cm}^{-3}$ , and a molecular hydrogen density of  $\sim 1 \times 10^5 \text{ cm}^{-3}$ . Further, since the (2, 2) line emission is optically thin, the total mass of molecular gas can be derived from the velocity-integrated flux density. Using the observed values of  $S(2, 2; m) = 74 \text{ mJy}$  and  $\Delta v = 5.5 \text{ km s}^{-1}$ , and the adopted parameters  $[\text{NH}_3/\text{H}_2] = 2 \times 10^{-7}$  and  $T_{\text{ex}} = T_K = 30 \text{ K}$ , we derive a molecular mass for the southwestern clump of  $\sim 4 M_\odot$ .

#### 4.3. The Relationship between the Ionized and Molecular Gas

In this section we examine the spatial distribution of the molecular gas relative to the ionized gas in G19.6–0.2 and discuss their possible physical relationship. The projected distribution on the plane of the sky of the ionized gas and of the molecular gas toward G19.6–0.2 is illustrated in Figure 9, which shows the radio continuum map at 1.6 GHz (resolution of  $\sim 1''.\text{5}$ ) projected on the velocity-integrated ammonia map (resolution of  $\sim 3''.\text{0}$ ). The ammonia emission detected with the VLA lies within a projected region that

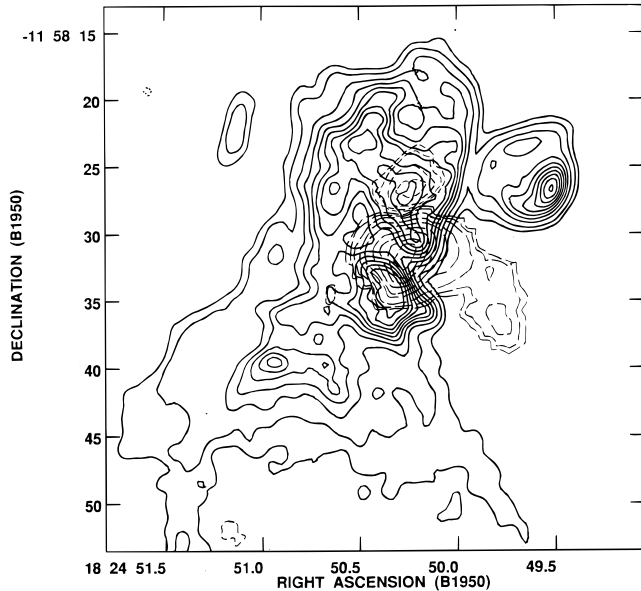


FIG. 9.—Map of the velocity-integrated emission in the main hyperfine line of the (2, 2) inversion transition (dashed lines), at  $3.^{\circ}4 \times 2.^{\circ}4$  angular resolution, superposed on a map of the 1.6 GHz continuum emission (solid lines), at  $1.^{\circ}5 \times 1.^{\circ}2$  angular resolution.

encompasses the cometary and northern regions of ionized gas.

The northern ammonia clump, detected in absorption in the (2, 2) main HF transition, is projected toward the northern region of ionized gas (component CD), implying that the H II region is behind the molecular gas. The systemic velocity of the northern ammonia clump ( $45.1 \text{ km s}^{-1}$ ) is similar to the systemic velocity of the ionized component ( $44.3 \text{ km s}^{-1}$ ), suggesting that the molecular structure is most likely physically associated with the ionized region. The molecular-line absorption probably arises from small subclumps located either within or at the boundary of the H II region. This hypothesis is supported by the highly clumpy structure of the northern H II region, which can be understood in terms of ionization of a primordial medium with large density inhomogeneities. The presence of clumps near recently formed stars might be a by-product of the fragmentation process that took place during the gravitational collapse. The denser clumps are more difficult to destroy by the ionization front than the interclump medium and will remain in the form of partially ionized globules for times considerably longer than the dynamical age of the H II region.

The ammonia emission from the middle clump is found projected toward both the bright cometary-like H II region and region F. Its peak position lies roughly between the positions of these two ionized sources. Since it is close to the middle clump and has a large luminosity ( $5.3 \times 10^4 L_{\odot}$ ), the radiation from the star that ionizes the cometary H II region is a primary candidate for the energy source that heats the middle clump. The stellar radiation most likely heats the dust that in turn heats the gas through dust-gas collisions. To assess this hypothesis quantitatively, although in an approximate manner, we assume that the total luminosity emitted by the middle clump, mostly in the form of infrared emission from dust, can be approximated by that of a blackbody with a (dust) temperature of 30 K and an angular diameter of  $2.^{\circ}7$ . We derive the luminosity of the middle

clump to be  $\sim 2 \times 10^3 L_{\odot}$ . The solid angle  $\Omega$  subtended by the middle clump from the exciting star is approximately  $\pi(\theta_s/\theta_L)^2/4$ , where  $\theta_s$  is the clump angular diameter, and  $\theta_L$  is the angular distance between the star and the clump. Assuming that the exciting star is at the focus of the cometary-like structure, we derive  $\Omega \sim 0.44 \text{ sr}$ , so that the required exciting luminosity is  $5.7 \times 10^4 L_{\odot}$ . We conclude that the radiation field from the O8.5 ZAMS star (see Table 5) is the main source responsible for heating the middle clump gas.

The emission from the middle clump might originate solely from shocked material in the swept-up shell behind the shock front driven by the expansion of the nearby cometary H II region. A quantitative evaluation of this hypothesis shows that while the observed density of the middle clump of  $9 \times 10^6 \text{ cm}^{-3}$  could be explained by the compression produced by the shock driven by the expansion of the H II region, the predicted thickness of the molecular swept-up shell (see, Keto & Ho 1989) is more than an order of magnitude smaller than the observed thickness. We suggest that the ammonia middle clump is part of a relatively more extended and less dense preexisting molecular cloud within the G19.6–0.2 region. The cloud is possibly a relic of the process of collapse and fragmentation of a large molecular cloud that led to the formation of a cluster of massive stars. The ammonia emission from the middle clump originates in the gas that has been heated and compressed, and thus lighted up, by the action of a young luminous star recently formed at the southern edge of the molecular cloud. The physical association between the middle clump and the ionized region A is envisioned as follows: The cometary H II region is thought to be ionized by a star that was born near the boundary of the molecular cloud and is currently undergoing expansion in a medium with strong density gradients. The systemic radial velocity of the cometary H II region ( $36.9 \text{ km s}^{-1}$ ) is blueshifted by  $3.5 \text{ km s}^{-1}$  relative to the systemic radial velocity of the dense molecular clump ( $40.4 \text{ km s}^{-1}$ ). Since the (2, 2) NH<sub>3</sub> line is not seen in absorption toward source A, the ionized gas probably lies in front of the clump. These observations strongly support the hypothesis that source A is experiencing a champagne phase of evolution (see Yorke, Tenorio-Tagle, & Bodenheimer 1983); that is, it is expanding away from the dense molecular cloud. The shock front driven by the expansion of the H II region in the direction of increasing density (i.e., toward the central region of the cloud) compresses the gas, further enhancing its density and creating the densest region within the cloud (the middle clump). In addition, we suggest that the low-density blueshifted (outflowing) molecular gas detected toward the middle clump (see § 3.3) also may have originated at this stage of evolution, and thus corresponds to molecular gas from the cloud that is driven and dispersed by the champagne flow from the cometary H II region.

The broad line width of the ammonia emission from the middle clump needs an explanation. The kinetic temperature ( $\sim 30 \text{ K}$ ) and line width of the ammonia emission ( $6.6 \text{ km s}^{-1}$  in the satellite lines) implies that the motions within the clump are primarily nonthermal. As a result of insufficient spatial resolution, the physical origin of the non-thermal motions is difficult to establish. Does the line width reflect gravitationally bound motions of the middle clump? Assuming that the clump is in virial equilibrium, we derive a virial mass of  $210 M_{\odot}$  from the observed values of the radius of  $0.023 \text{ pc}$  and line width of  $6.6 \text{ km s}^{-1}$ . This mass is

~8 times larger than that derived from the observed ammonia column density, based on an [NH<sub>3</sub>/H<sub>2</sub>] abundance ratio of  $2 \times 10^{-7}$  (see § 4.2.1). An abundance ratio of  $2 \times 10^{-8}$  is required to bring these two masses into agreement. Although we cannot rule out this possibility, it is more likely that the middle clump is not in equilibrium, but is undergoing expansive motions produced by either the nearby stars or an embedded star in the process of formation. The most likely explanation for the line width is that the shock driven by the cometary H II region into the middle clump is accelerating the molecular gas and broadening the ammonia line. It is even possible that part of the gas within the middle clump may have been pushed into collapse by the encroaching shock. The observed spatial distribution and kinematics of the OH maser features within G19.6–0.2 provide additional information. The OH maser emission arises from several spots confined within a region small in angular size (~1" in diameter), which is coincident with the peak position of the middle ammonia clump. The radial velocities of the maser spots have an average value of 41.2 km s<sup>-1</sup>, similar to the radial velocity of the middle clump ( $40.4 \pm 0.9$  km s<sup>-1</sup>), and cover a range of 5.5 km s<sup>-1</sup> (GRM), similar to the line width of the ammonia emission from the clump structure. This suggests that the OH maser cloudlets share the motions of the molecular gas within the middle clump.

Alternatively, it is possible that the middle clump harbors a young object that is undergoing strong mass loss, and has enough mechanical luminosity to alter the motions of its surroundings, but not enough to ionize an appreciable amount of gas. The clump material would then be tracing the outflow of matter in the last stages of the formation of a star. Estimating the outflow velocity  $V_0$  as  $\Delta v/2$ , the flow lifetime  $\tau$  as  $R/V_0$ , and the flow mechanical luminosity  $L_m$  as  $\frac{1}{2}MV_0^2/\tau$ , where  $\Delta v$ ,  $R$ , and  $M$  are, respectively, the line width, radius, and mass of the clump, we find  $V_0 \sim 3.3$  km s<sup>-1</sup>,  $\tau \sim 7 \times 10^3$  yr, and  $L_m \sim 0.7 L_\odot$ . The corresponding mass-loss rate is  $\sim 7 \times 10^{-4} M_\odot$  yr<sup>-1</sup>.

The southwestern ammonia clump is not directly associated with a radio continuum source. However, its morphology is roughly elongated following the northwestern edge of the largest shell-like ionized structure within G19.6–0.2 (see Fig. 9), which could indicate an association. The line width of the ammonia emission, 5.5 km s<sup>-1</sup>, is considerably larger than the thermal widths, implying that nonthermal motions are dominant. Assuming the gas is in virial equilibrium, we obtain a virial mass of  $\sim 270 M_\odot$ , about 70 times greater than the mass derived from the observed flux density in the (2, 2) line. We conclude that the southwestern clump is not in virial equilibrium, and suggest that its molecular emission arises from the compressed and heated gas behind the shock front driven by the expansion of the largest H II regions within G19.6–0.2. Structures of molecular gas immediately surrounding extended regions of ionized gas, such as this one, may represent the latest stage in the evolution of a warm molecular core before it is disrupted by the expansion of the large H II regions.

#### 4.4. Massive-Star Formation within a Massive Molecular Core

We propose that the G19.6–0.2 region corresponds to a massive (a few times  $10^3 M_\odot$ ) molecular core with a size of about 1 pc in which massive stars have formed recently. It is not clear, however, how the interstellar gas is organized into

massive molecular cores, nor how the collapse of dense molecular cores leads to the formation of massive stars in associations. We suggest that at an earlier stage of evolution, possibly as the result of the initial collapse and fragmentation of a large molecular cloud, the G19.6–0.2 core consisted of several dense clumps with a power-law mass spectrum and a less dense interclump medium (see Blitz 1991, and references therein). The ensuing collapse of the most massive molecular clouds probably gave rise to the most massive (and luminous) O stars that, in turn, rapidly ionized their surroundings, thus creating the H II regions. If we postulate that the systemic motions of the H II regions are dynamically coupled to a massive molecular core of mass  $M_c$ , then the mass required to bind the motions is

$$M_c \sim \frac{3R\langle v_r^2 \rangle}{G},$$

where  $\langle v_r^2 \rangle^{1/2}$  is the velocity dispersion in the radial direction, and  $R$  is a typical distance from the H II regions to the center of mass. Using the observed dispersion 3.3 km s<sup>-1</sup> in the radial velocities of the H II regions (see Table 3), and estimating  $R$  from Figure 4 as  $\sim 0.2$  pc, we obtain  $M_c \sim 1.5 \times 10^3 M_\odot$ . The average molecular density in a region that is 0.5 pc in radius is then  $\sim 5 \times 10^4$  cm<sup>-3</sup>. From observations at 1.3 mm, Chini et al. (1987) estimated that the total mass of gas within the G19.6–0.2 region is  $\sim 6 \times 10^3 M_\odot$  (corrected to the adopted distance of 3.5 kpc), which supports our model. We note that the predicted density of the molecular gas is large, and single-dish observations of molecular transitions with large critical densities could confirm (or negate) these mass estimates.

The question of whether all of the H II regions were formed closely in time is difficult to answer. For the more extended H II regions (components CD and E) we estimate, using the sizes of the shell-like features associated with them (radii between 0.1 and 0.2 pc), that they have dynamical ages of  $\sim 3-6 \times 10^4$  yr. We suggest that the stars exciting these H II regions may have been formed in the first episode of star formation within the G19.6–0.2 core. The large pressure exerted by the radiation, ionization fronts, and winds from the first generation of stars may have then triggered a further generation of massive stars, which gave rise to the compact H II regions A and B. In particular, the cometary-like H II region, which has a dynamical age of  $\sim 2 \times 10^3$  yr, lies right at the edge of the largest arc-shaped ionization front associated with source E, and hence its formation may have also been induced by the compression of a massive molecular clump by the shock moving ahead of the arc-shaped ionization front. The most compact region within the ionized complex, source F, also has a dynamical age of  $\sim 2 \times 10^3$  yr. This dynamical timescale, however, may not provide a realistic estimate of the actual age of H II region F. Owing to the high density of the molecular gas in which it is embedded (middle clump), it is possible that region F is in pressure equilibrium with the dense surroundings, and currently stalled at its equilibrium radius (De Pree, Rodríguez, & Goss 1995). Assuming that the density and temperature of the ambient medium are  $9 \times 10^6$  cm<sup>-3</sup> and 30 K, respectively, we find that the final equilibrium radius of source F ( $N_i = 1.9 \times 10^{47}$  s<sup>-1</sup>) is  $\sim 0.03$  pc, close to the observed radius of  $\sim 0.02$  pc, which suggests that object F may be pressure confined by the dense environment.

After massive stars are born in a clumpy molecular cloud, their environment should suffer a profound impact. The clumps that become exposed to the ionizing radiation will begin to photoevaporate. Under certain conditions the ionization-shock compression could implode a clump, thereby triggering the formation of a star (Klein, Sandford, & Whitaker 1983; Bertoldi 1989; Bertoldi & McKee 1992). We think that the dense molecular structures within G19.6–0.2 delineate the molecular gas within the core that has been influenced by the dynamical effects of the stellar wind and expansion of the H II regions. Most of these molecular structures will probably be transient, but some may be massive and dense enough to be gravitationally bound. In particular, we argued in § 4.3 that the motions within the southwestern clump are probably produced by shocks driven by the expansion of the first generation of H II regions. The ammonia middle clump is thought to be the remnant of a dense cloud of molecular gas that is in the process of being compressed by the radiation from the nearby recently formed (second-generation) massive star. The cloud itself is probably the result of the large-scale collapse of a molecular cloud that led to the formation of several dense clumps with a power-law mass spectrum, several of which already have been photoevaporated by the radiation from the first generation of massive stars.

We suggest that the G19.6–0.2 region, containing a cluster of OB stars and dense molecular clumps, is the result of the process of collapse and fragmentation of a massive molecular core. The first generation of luminous stars, which should have eventually formed from the denser and most massive primordial clumps, led to the formation of the more diffuse H II regions (now seen as components CD and E). The winds and ionizing shocks from these stars led to the disruption of the less dense primordial clumps and triggered the formation of a new generation of massive stars from the most massive of the remaining clumps. The second generation of stars then gave rise to the compact H II regions (components A, B, and F). The middle clump is currently experiencing the effects from a second-generation star; that is, it is undergoing heating by the radiation from the star exciting source A, and being compressed by the shock of its associated H II region. It is even possible that the middle clump may have become dynamically unstable by these effects and is undergoing the formation of a star at its center. This molecular clump thus may be the progenitor of a third generation of stars. Molecular clumps in a similar evolutionary stage already have been proposed to be present, in other massive-star-forming regions, by Wilson, Gaume, & Johnston (1993) and by Olmi et al. (1993).

## 5. SUMMARY

We observed the H66 $\alpha$  recombination line, the NH<sub>3</sub> (2, 2) inversion transition line, and the 1.6 GHz radio continuum emission toward the G19.6–0.2 star-forming region with the VLA at angular resolutions of 2"–3". The main results of the observations and conclusions presented in this paper are summarized as follows.

The radio continuum observations show that the ionized gas has a complex appearance. We detected, in a region ~0.8 pc in diameter, five distinct components with sizes ranging from 0.03 to 0.4 pc. The three largest ones exhibit ring- or shell-like structures and have clumpy and inhomogeneous distributions of gas. The brightest compact H II

region within the complex shows a cometary-like morphology, which may be due to the expansion of ionized gas in an anisotropic medium. The H66 $\alpha$  radio recombination line observations show that the different components of ionized gas have different line-center velocities. The velocity dispersion is 3.3 km s<sup>-1</sup>, which, if it is due to gravitationally bound motions of the H II regions, implies a mass of  $\sim 1.5 \times 10^3 M_\odot$  inside a region of ~0.4 pc in radius. These continuum and recombination line observations indicate the presence of five distinct H II regions that are excited by individual stars, implying that the G19.6–0.2 region corresponds to a region where a cluster of massive O and B stars has been recently formed. Some of the ultracompact structures detected with higher angular resolution (~0.4") toward these H II regions probably correspond to partially ionized clumps, which are externally ionized and embedded within the larger H II regions.

The NH<sub>3</sub> (2, 2) line observations show that the molecular emission arises from three distinct structures within a region of ~0.3 pc in diameter, located near the center of the cluster of H II regions. The northern clump, detected in absorption toward the northernmost H II region, has a velocity of 45.1 km s<sup>-1</sup> and a density of  $\sim 2 \times 10^5 \text{ cm}^{-3}$ . The southwestern clump has a velocity of 41.8 km s<sup>-1</sup> and a density of  $\sim 1 \times 10^5 \text{ cm}^{-3}$ . The densest and brightest ammonia structure, the middle clump, has a size of ~0.05 pc, a density of  $\sim 9 \times 10^6 \text{ cm}^{-3}$ , and exhibits very broad line widths (~9.5 km s<sup>-1</sup>). It is intimately associated with the cometary-like and the most compact H II regions within the complex. We suggest that the middle clump is heated by the radiation from the recently formed luminous star that excites the cometary H II region, and is compressed by the shock front driven by the expansion of the ionized gas into the clump. The broad line width of the ammonia emission is probably due to expansion motions produced by this shock.

We suggest that the G19.6–0.2 region, containing a cluster of OB stars and dense molecular clumps, is the result of the process of collapse and fragmentation of a massive (a few times  $10^3 M_\odot$ ) molecular core, which initially led to the formation of a hierarchy of molecular clumps. The massive stars exciting the largest H II regions may have been formed first, presumably from the denser and most massive molecular substructures. The pressure exerted by the radiation and winds from these stars may have then compressed nearby clumps and triggered the formation of a new generation of massive stars. The middle molecular clump is thought to be a remnant core within the G19.6–0.2 region, possibly a relic of the process of large-scale collapse and fragmentation of a large molecular cloud that led to the formation of a cluster of massive stars. We suggest that the star that excites the cometary H II region was formed at the edge of the middle clump. The ionized gas flowing toward the observer is undergoing expansion into the lower density interclump medium (champagne flow). In the opposite direction, the H II region drives a shock into the dense molecular clump, compressing it and further increasing its density.

We thank P. T. P. Ho for providing us with the VLA continuum observations of G19.6–0.2 at 4.9 GHz. G. G. gratefully acknowledges support from the Visiting Scientist Fund of the Smithsonian Institution, from a Guggenheim Fellowship, and from the Chilean FONDECYT (project 1950524).

## REFERENCES

- Beichman, C. A., Becklin, E. E., & Wynn-Williams, C. G. 1979, *ApJ*, 232, L47  
 Bertoldi, F. 1989, *ApJ*, 346, 735  
 Bertoldi, F., & McKee, C. F. 1992, *ApJ*, 395, 140  
 Blitz, L. 1991, in *The Physics of Star Formation and Early Stellar Evolution*, ed. C. J. Lada & N. D. Kylafis (Dordrecht: Kluwer), 3  
 Brand, J. 1986, Ph.D. thesis, Univ. Leiden  
 Brown, R. L., Lockman, F. J., & Knapp, G. R. 1978, *ARA&A*, 16, 445  
 Cesaroni, R., Churchwell, E., Hofner, P., Walmsley, C. M., & Kurtz, S. 1994, *A&A*, 288, 903  
 Cesaroni, R., Walmsley, C. M., & Churchwell, E. 1992, *A&A*, 256, 618  
 Chini, R., Kreysa, E., Mezger, P. G., & Gemünd, H.-P. 1986, *A&A*, 154, L8  
 Chini, R., Krügel, E., & Wargau, W. 1987, *A&A*, 181, 378  
 Churchwell, E. 1990, *A&A Rev.*, 2, 79  
 Churchwell, E., Walmsley, C. M., & Cesaroni, R. 1990, *A&AS*, 83, 119 (CWC)  
 De Pree, C. G., Rodríguez, L. F., & Goss, W. M. 1995, *ApJ*, 447, 220  
 Garay, G., Lizano, S., & Gómez, Y. 1994, *ApJ*, 429, 268  
 Garay, G., Reid, M. J., & Moran, J. M. 1985, *ApJ*, 289, 681 (GRM)  
 Garay, G., & Rodriguez, L. F. 1990, *ApJ*, 362, 191  
 Genzel, R., & Downes, D. 1977, *A&AS*, 30, 145  
 Genzel, R., Downes, D., Ho, P. T. P., & Bieging, J. 1982, *ApJ*, 259, L103  
 Gómez, Y., Garay, G., & Lizano, S. 1995, *ApJ*, 453, 727  
 Habing, H. J., & Israel, F. P. 1979, *ARA&A*, 17, 345  
 Henkel, C., Wilson, T. L., & Mauersberger, R. 1987, *A&A*, 182, 137  
 Ho, P. T. P., & Haschick, A. D. 1981, *ApJ*, 248, 622  
 Ho, P. T. P., & Townes, C. 1983, *ARA&A*, 21, 239  
 Keto, E. R., & Ho, P. T. P. 1989, *ApJ*, 347, 349  
 Klein, R. I., Sandford, M. T., II, & Whitaker, R. W. 1983, *ApJ*, 271, L69  
 Kurtz, S., Churchwell, E., & Wood, D. O. S. 1994, *ApJS*, 91, 659  
 Lizano, S., Cantó, J., Garay, G., & Hollenbach, D. 1996, *ApJ*, 468, 739  
 Mauersberger, R., Henkel, C., Wilson, T. L., & Walmsley, C. M. 1986, *A&A*, 162, 199  
 Olmi, L., Cesaroni, R., & Walmsley, C. M. 1993, *A&A*, 276, 489  
 Plume, R., Jaffe, D. T., & Evans, N. J., II. 1992, *ApJS*, 78, 505  
 Reid, M. J., & Moran, J. M. 1981, *ARA&A*, 19, 231  
 Reid, M. J., Myers, P. C., & Bieging, J. H. 1987, *ApJ*, 312, 830  
 Schwab, F. 1980, *Proc. SPIE*, 231, 18  
 Walmsley, C. M. 1989, in *Evolution of Interstellar Dust and Related Topics*, ed. A. Bonetti, J. M. Greenberg, & S. Aiello (Amsterdam: Elsevier), 179  
 ———. 1992, in *Chemistry and Spectroscopy of Interstellar Molecules*, ed. D. K. Bohme et al. (Tokyo: Univ. Tokyo), 267  
 Wilson, T. L., Gaume, R. A., & Johnston, K. J. 1993, *ApJ*, 402, 230  
 Wood, D. O. S., & Churchwell, E. 1989, *ApJS*, 69, 831 (WC)  
 Yorke, H. W., Tenorio-Tagle, G., & Bodenheimer, P. 1983, *A&A*, 127, 313